Nucleic Acids Research, 2023, **51**, 12031–12042
https://doi.org/10.1093/nar/gkad1002
Advance access publication date: 11 November 2023
Chemical Biology and Nucleic Acid Chemistry

Uridine–cytidine kinase 2 potentiates the mutagenic influence of the antiviral β-d-N4-hydroxycytidine

Zhen Xu[1,2], Christoffer Flensburg[1,2], Rebecca A. Bilardi[1,2] and Ian J. Majewski[1,2,*]

[1]The Walter and Eliza Hall Institute of Medical Research, 1G Royal Parade, VIC 3052, Australia
[2]University of Melbourne, Department of Medical Biology, 1G Royal Parade, VIC 3052, Australia
[*]To whom correspondence should be addressed. Tel: +61 3 9345 2555; Fax: +61 3 9347 0852; Email: majewski@wehi.edu.au

Abstract

Molnupiravir (EIDD-2801) is an antiviral that received approval for the treatment of severe acute respiratory syndrome coronavirus 2 (SARS-CoV2) infection. Treatment of bacteria or cell lines with the active form of molnupiravir, β-d-N4-hydroxycytidine (NHC, or EIDD-1931), induces mutations in DNA. Yet these results contrast *in vivo* genotoxicity studies conducted during registration of the drug. Using a CRISPR screen, we found that inactivating the pyrimidine salvage pathway component uridine–cytidine kinase 2 (Uck2) renders cells more tolerant of NHC. Short-term exposure to NHC increased the mutation rate in a mouse myeloid cell line, with most mutations being T:A to C:G transitions. Inactivating Uck2 impaired the mutagenic activity of NHC, whereas over-expression of Uck2 enhanced mutagenesis. UCK2 is upregulated in many cancers and cell lines. Our results suggest differences in ribonucleoside metabolism contribute to the variable mutagenicity of NHC observed in cancer cell lines and primary tissues.

Graphical abstract

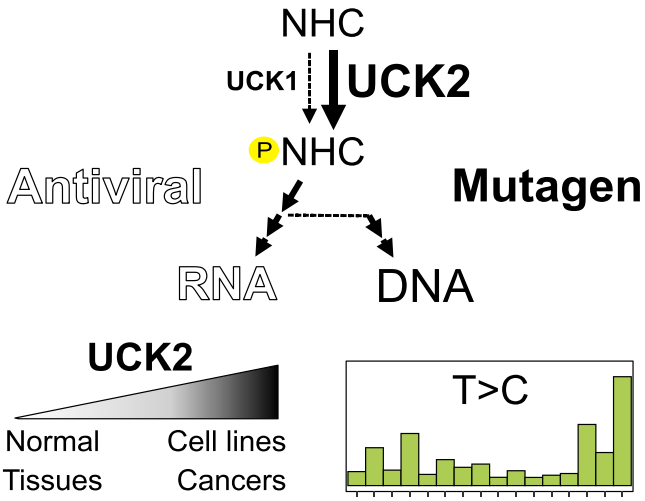

Introduction

Nucleoside and ribonucleoside analogs are important therapeutics that have found application both in the treatment of cancer and as antivirals. Molnupiravir is a broad spectrum anti-viral that has been deployed as a treatment for SARS-CoV2 infection. Clinical trials to assess the efficacy of molnupiravir are ongoing; however, several groups have reported that early treatment with the drug aids clearance of the virus (1,2). More recent trials carried out in largely vaccinated populations suggest that molnupiravir does not reduce SARS-CoV2-associated hospitalisations or deaths (3). Molnupiravir is metabolised in the body to its active form β-d-N4-hydroxycytidine (NHC or EIDD-1931) (4). The triphosphate form of NHC is incorporated into viral RNA during replication and induces mutations by base pairing variably, acting either like cytidine or uridine (5). Mutagenesis of the viral genome has been confirmed with human coronaviruses in experimental models and by sequencing clinical isolates from people infected with SARS-CoV2 who had been treated with molnupiravir (5–8).

More recently there has been debate around the potential for molnupiravir to induce mutations in the human genome (reviewed by Waters *et al.* (9)). It seems clear that treatment of bacteria, or human or mouse cell lines with molnupiravir induces mutations in DNA. Most recently, high sensitivity genome sequencing confirmed that short-term treatment with

Received: June 7, 2023. **Revised:** October 11, 2023. **Editorial Decision:** October 12, 2023. **Accepted:** October 19, 2023
© The Author(s) 2023. Published by Oxford University Press on behalf of Nucleic Acids Research.
This is an Open Access article distributed under the terms of the Creative Commons Attribution-NonCommercial License (http://creativecommons.org/licenses/by-nc/4.0/), which permits non-commercial re-use, distribution, and reproduction in any medium, provided the original work is properly cited. For commercial re-use, please contact journals.permissions@oup.com

molnupiravir or NHC was sufficient to induce an excess of T:A to C:G transitions in two cell lines, one murine and one human (10). This result built on an earlier finding that extended culture of cells in NHC resulted in higher rates of resistance to 6-thioguanine treatment in a modified form of the *HPRT* assay (11). Yet, these studies stand in contrast to *in vivo* genotoxicity studies performed as part of the drug registration that suggest the drug is safe and not mutagenic (12,13). In those studies, rats were treated with high doses of molnupiravir and mutation rates were assessed with the *Pig-a* red cell phenotyping assay or the Big Blue® (cII Locus) transgene and found to be within the range of historical negative controls. Similarly the results of fertility and fetal development studies in rats and rabbits identified toxicity issues at high doses, but they do not support the contention that the drug acts as a potent mutagen. As is appropriate for an emerging therapy, molnupiravir is not recommended for use during pregnancy and is subject to an ongoing safety assessment.

We set out to define genetic factors that modify cellular responses to molnupiravir. Using an unbiased genome-wide CRISPR-Cas9 screen we found inactivation of genes involved in the DNA damage response, cell death and the pyrimidine salvage pathway promoted resistance to NHC in mouse *Eμ-Myc* B lymphoma cell lines. Uridine-cytidine kinases (UCK1 and UCK2) phosphorylate the ribonucleosides uridine and cytidine and act as the rate limiting step in the pyrimidine salvage pathway (14). Pyrimidine salvage is commonly up-regulated in cancers and this is often attributed to higher levels of UCK2 (14). UCK2 can phosphorylate a variety of ribonucleoside analogs and this capacity has been used as a strategy to target cancer cells with toxic analogs (reviewed in (15)). We found that manipulating the expression of Uck2 modulates both the toxicity and mutagenicity of NHC in cell lines. The restricted expression of Uck2 in normal tissues may explain the variable mutagenicity of molnupiravir and NHC in exposure models. These results raise important questions about how we evaluate mutagenicity of emerging drugs and whether there are cells within the body that are susceptible to mutagenesis because of differences in metabolic activity.

Materials and methods

Cell lines and viability assays

Eμ-Myc mouse lymphoma and HoxA9-Meis1-transformed mouse acute myeloid leukaemia cell lines were generated and cultured as previously described (16,17). *Eμ-Myc* lymphoma cell lines (#AH15A, AF47A) were cultured in high-glucose Dulbecco's modified Eagle's medium supplemented with 10% fetal bovine serum (FBS), 50 μM β-mercapto-ethanol and 100 mM asparagine. HoxA9-Meis1 myeloid cells were grown in DMEM with 10% FBS and murine IL-3 (10 ng/ml). Both cell lines were maintained at 37°C in 10% CO_2 and regularly verified as mycoplasma negative. For drug sensitivity assays, *Eμ-Myc* lymphoma cells or Hoxa9-Meis1 myeloid cells, or their derivatives, were seeded into white 96-well plates (Greiner, 655083) at a density of 5×10^4 cells/well and treated with drugs (typically 0–10 μM, 5-point serial dilution 1:4), including EIDD-1931 (S0833, SelleckChem), azacitidine (S1782, SelleckChem) and decitabine (S1200, SelleckChem). Cell viability was assessed at 48 h using CellTiter-Glo 2.0 Cell Viability Assay (Promega, G9241).

Cell counting

HoxA9-Meis1 cells were seeded into 12-well flat bottom plates at 3×10^4/ml in culture medium with or without 1 μM EIDD-1931. Cells were cultured for 8 days and counted using a flow cytometer. Briefly, 180 μl of cell culture was mixed with 20 μl of allophycocyanin-conjugated beads (3×10^5/ml) (340487, BD Biosciences) with 1 μg/ml propidium iodide (PI) (P4864, Sigma-Aldrich). Cell and bead counts were determined using an LSRFortessa Flow Cytometer (BD). Cells were passaged before becoming fully confluent and this dilution was considered when calculating the total viable cell number. Viable cell counts were expressed relative to the starting cell count (measured at day zero) to address any difference in the number of cells that were seeded.

Immunoblotting/antibodies

Eμ-Myc lymphoma or HoxA9-Meis1 myeloid cells were lysed in ONYX lysis buffer (50 mM Tris/HCl pH 7.5, 150 mM NaCl, 1% Triton X-100, cOmplete™ protease inhibitor cocktail, Roche) for 30 min on ice with occasional vortex, or directly in LDS sample buffer (NP0007, ThermoFisher) for 1 min at room temperature. Protein quantification was performed using the Bradford protein assay (Bio-Rad). Protein (50 μg per lane) was separated on pre-cast 4–12% SDS gradient gels (NuPAGE, Thermo Fisher) by SDS-PAGE and transferred to nitrocellulose membranes using the iBlot2 Gel transfer Device (Thermo Fisher). The membranes were blocked in 5% skim milk in PBST buffer (PBS with 0.1% Tween-20) for 1 h at room temperature, followed by incubation at 4°C overnight with antibodies: rabbit anti-Uck2 (proteintech, 10511-1-AP) and mouse anti-HSP70 (clone N6, a gift from Dr R Anderson, Peter MacCallum Cancer Centre, Melbourne). HRP conjugated goat anti-mouse IgG and goat anti-rabbit IgG (Southern Biotech) were used as secondary antibodies. Membranes were finally incubated in Luminata Forte Western HRP Substrate (Millipore, USA) for 2–5 min and scanned using the ChemiDoc MP Imaging System (BioRad). Images were merged to allow for visualisation of the molecular weight standards.

Genome-wide CRISPR/Cas9 knockout screen

The Genome-wide Mouse Lentiviral CRISPR gRNA Library v1 was used for our screen (Addgene, Pooled Library #50947) (18). To prepare the lentivirus, 1.5 μg of the library plasmid was used for co-transfection with packaging plasmids (1 μg pCMV-Rev (Addgene 115776), 1.5 μg pMDLg/pRRE (Addgene 12251), 1 μg pCMV-VSV-G (Addgene 8454)) for each 10 cm dish of HEK293T using 24 μl FuGENE HD Transfection Reagent (Promega, E2311). Ten dishes of HEK293T cells were used to achieve a good representation of each sgRNA. Supernatants were harvested 48 h post transfection, combined, passed through a 0.22 μM filter and aliquoted.

Two independent Cas9-mCherry expressing *Eμ-Myc* cell lines were generated for this screen. Cas9 lentivirus was prepared using FUCas9-Cherry plasmid (Addgene 70182) using the same method above. For viral transduction, 1 ml of Cas9 viral supernatant was added to 1×10^6 WT cells in 3 ml of complete media with polybrene (4 mg/ml) (Sigma, H9268). The cell-virus mixture was centrifuged at 3000 rpm at room temperature for 1 h followed by incubation at 37°C overnight. After a minimum of two days in culture, viable mCherry positive cells were sorted on the FACSAria system (BD).

For each Cas9-mCherry expressing Eμ-*Myc* line, 5×10^7 cells were transduced with sgRNA library lentivirus and a transduction efficiency of ∼20% was achieved. Puromycin (1 μg/ml) was added to cells 48 h post transduction and maintained for 3 days to select for sgRNA expressing cells. To maintain a 100x representation for each sgRNA, 1×10^7 cells were collected for the baseline control (day 3). 5×10^7 cells were selected with 4 rounds of EIDD-1931 treatment. For each round, cells were treated with 5 μM EIDD-1931 for 3 days and left untreated for 2–5 days for recovery and expansion. At the end of each round, 1×10^7 cells were collected. In parallel, another aliquot of 5×10^7 cells were left untreated and 1×10^7 cells were harvested at the end of experiment.

Genomic DNA was extracted from cell pellets using DNeasy Blood & Tissue Kits (Qiagen, 69506). Libraries were prepared using barcoded primers as previously described (19), then sequenced on the NextSeq platform (Illumina). To identify genes whose sgRNAs were enriched after EIDD-1931 treatment, the raw counts for each sgRNA were normalized to counts per million reads (CPM) and then $\log_2$ transformed. A LOWESS curve was fitted to the relationship between EIDD-1931 treated samples and baseline controls and residues were calculated for each sgRNA. sgRNAs were then sorted in descending order of their residual values, following by minimum hypergeometric *P* value calculation for each gene in the library using an established algorithm (20). These were subsequently converted to false discovery rate adjusted *P* values (*q* values). Lastly, genes were ranked by their q value.

Generation of knockout cell lines using CRISPR/Cas9 technology

The lentiviral-based CRISPR/Cas9 editing system has been described previously (18). Briefly, two independent sgRNA targeting mouse *Uck1* (GGATGACCAACTTGCGCTGC and TGTTGAAGGCAAAACTGTCG), *Uck2* (CAAAGTCG TACACGGGGATC and GCCGACGTGGTGCTCTTCGA), *Cmpk1* (AGTTCACCATACTGTGAGTC and TGGTCGT GTTCGTTTTGGGC) or mouse *Trp53* (19) were cloned into pKLV-U6gRNA (BbsI)-PGKpuro2ABFP (Addgene 50946). Lentivirus was prepared and Cas9-mCherry expressing *Eμ-Myc* lymphoma cells or HoxA9-Meis1 myeloid cells were transduced as described above. mCherry/BFP double positive cells were single-cell sorted into 96-well plates by FACS using FACSAria system (BD). Sequencing of genomic DNA from clonal cell lines using the Illumina MiSeq sequencing platform (San Diego, CA, USA) has been described (19)

γ-H2AX assays

Eμ-Myc lymphoma cells and HoxA9-Meis1 myeloid cells with varied *Uck2* expression levels were treated with the drugs indicated for 24 h. Cells were fixed and permeabilized with BD Cytofix/Cytoperm buffer (BD Biosciences, 51–2090KZ) for 30 min on ice, followed by Permeabilization Buffer Plus (BD Biosciences, 561651) for 10 min on ice and refixed with BD Cytofix/Cytoperm buffer for 5 min at room temperature. Permeabilized cells were resuspended in BD Perm/Wash buffer (BD Biosciences, 51-2091KZ) supplemented with AF647-conjugated antibodies to detect γ-H2AX (BD Biosciences, 560447, clone N1-431) or similarly labelled IgG1, κ isotype control antibodies (BD Biosciences, 557714), and stained by incubation for 60 min on ice. Cells were analysed using a LSR-Fortessa Flow Cytometer (BD) and the positive fraction determined by setting a gate on the WT parental control.

RNA sequencing and analysis

The use of mice was approved by the WEHI Animal Ethics Committee (Project 2020.021). RNA was extracted from primary tissues from C57BL/6 mice (bone marrow or liver) or from cell lines using the RNeasy Mini Kit (74104, Qiagen), then quantified using RNA ScreenTape on a 4200 TapeStation System (5067–5576, Agilent). Libraries were prepared using the TruSeq RNA Library Prep Kit v2 (RS-122–2001, RS-122–2002, Illumina) and sequenced using a paired end protocol (61 bases for each read) on a NextSeq2000 using NextSeq 1000/2000 P2 Reagents (100 cycle kit) v3 (20046811, Illumina). The data was aligned with STAR version 2.5.3 (21), deduplicated with Markduplicates version 3.1.0 (Picard Toolkit 2019, Broad Institute, GitHub Repository: https://broadinstitute.github.io/picard/) and counts generated with featureCounts (22). Transcripts per million (TPM) values were calculated for each gene.

EIDD-1931 treatment for mutation identification

WT, Uck2-deficient or Uck2 overexpressing HoxA9-Meis1 myeloid cell lines were generated to evaluate the mutagenicity of EIDD-1931 on genomic DNA. WT cells were single-cell sorted into 96-well plates and expanded for drug treatment. Uck2 null cells were generated using CRISPR-Cas9 editing, using the same method described above. To generate Uck2 overexpressing HoxA9-Meis1 cells, we first made a Uck2 expression construct with a mmUck2-3XFLAG synthesised gBlock (IDT). The DNA fragment was cloned into pMSCV-IRES-GFP plasmid using BglII and HpaI sites to generate pMSCV-mmUck2-3XFLAG-IRES-GFP. pMSCV-mmUck2-3XFLAG-IRES-GFP (3.6 μg) was then co-transfected with packaging plasmids (1.2 μg gag/pol (Addgene 14887) and 0.6 μg pCMV-VSV-G (Addgene 8454)) for each 10 cm dish of HEK293T using 27 μl FuGENE HD Transfection Reagent. HoxA9-Meis1 cells were transduced using the same method detailed above, except without Polybrene. Individual GFP positive cells were then sorted into 96-well plates and expanded.

Prior to the drug treatment, 1×10^6 cells were collected from the WT, Uck2-deficient and Uck2 overexpressing cell lines to serve as a reference for mutation calling. The cultures were then treated twice for a period of 4 days with 1 μM EIDD-1931 or DMSO, with a recovery period of 3 days between treatments. Single cells were sorted into 96-well plates and expanded, they were screened for Uck2 expression by immunoblotting and DNA was made for whole genome sequencing. Three clones were selected from each treatment (EIDD-1931 or DMSO) for each cell line for genome sequencing.

Genome sequencing and analysis

Genomic DNA was extracted from single cell clones using the DNeasy Blood and Tissue Kit (Qiagen) and quantified using the Genomic DNA ScreenTape on the 4200 TapeStation (Agilent). Genomic libraries were generated using the TruSeq DNA kit (Illumina) after shearing on the Covaris (Covaris). Pooled libraries were sequenced on a NovaSeq (Illumina) at the Australian Genome Research Facility using a 150-bp paired-end protocol, generating between 206–560 million reads per sample.

Genome sequencing reads were aligned to the mouse genome (mm10) using BWA-MEM (version 0.7.17-r1188) and deduplicated (23). Variant calling was performed within SuperFreq (version 1.4.4) (24) using Varscan 2 (version 2.3) (25). A series of mouse genomes were used as reference normal samples, including BALB/cJ, C57BL/10J, C57BL/6NJ, CAST/EiJ and NZO/HILtJ (26). In addition, a pre-exposure sample was included for each cell line to define somatic variants. Somatic variants were selected based on the somaticP score in SuperFreq (>0.1), minimum read depth (15) and variant allele frequency (VAF > 0.3). Variants were removed if they were detected in any other sample, or if they appeared in simple repeats or low complexity regions classified with RepeatMasker (http://www.repeatmasker.org). The mutation rate (mutations/Mbp) was calculated by dividing the number of mutations by the number of base pairs with read depth of 15 or more, excluding the filtered repeat and low complexity regions. Mutational signatures were plotted and analysed using MutationalPatterns (27). Three samples showed evidence of oxidative damage during library preparation (28), but these variants were excluded due to their low VAF.

We isolated an EIDD-1931 associated signature (e) using mutation calls from wildtype HoxA9-Meis1 cell lines, which involved subtracting a background signature evident in cells treated with vehicle (DMSO). In this case, we performed a subtraction after projecting the treated signature onto the background signature: $e = t - b\frac{t \cdot b}{\|b\|^2}$ where t is the average signature of the EIDD-1931 treated samples, b is the average signature of the DMSO treated samples and $t \cdot b$ is the scalar product. Negative signature elements were replaced with 0. The same subtraction approach was used for the reanalysis of published data from L5178Y and TK6 cell lines (10). A non-negative matrix factorisation was also performed across all HoxA9-Meis1 samples to identify signatures *de novo* (27,29). Mutations were decomposed into the background and EIDD-1931 signatures using non-negative least-square optimisation.

Drug safety evaluation data

Data regarding the drug safety evaluation of molnupiravir (Lagevrio) was gathered from public registration data presented to the United States Federal Drug Administration (https://www.fda.gov/media/154418/download) and the United Kingdom Medicines and Healthcare products Regulatory Agency (https://assets.publishing.service.gov.uk/government/uploads/system/uploads/attachment_data/file/1112678/Lagevrio_200_mg_hard_capsules_PLGB_53095_0089_APPROVEDPUB.pdf).

Statistical analysis

Statistical analysis of the CRISPR screen is detailed above. Details regarding replicates and error bars are included in the figure legends and in supplementary data. Absolute IC_{50} values and error estimates were calculated from viability assays using 'Nonlinear regression (curve fit)'—'Dose–Response'—'Special, X is log (concentration)'–'Absolute IC_{50}, X is log (concentration)'method in Prism9 software, the baseline was set as 0. If an IC_{50} value could not be calculated it was marked as not determined and the maximum tested dose noted. Summary level statistics including geometric mean and 95% confidence intervals were calculated at the level of each experiment to allow comparison between groups. For comparison of mutation rates, we used Prism9 software to perform a one-way ANOVA and then compared selected groups using Sidak's multiple comparison test with Bonferroni correction for multiple testing.

Results

Identifying genes that modulate response to EIDD-1931

We examined the effect of NHC/EIDD-1931 treatment on mouse haematopoietic cancer cell lines, including those derived from *Eμ-Myc* lymphomas and HoxA9-Meis1 transformed myeloid cells (17,30). We assessed the impact of EIDD-1931 on cell survival and proliferation with CellTiter-Glo, using two independent cell lines for each model. EIDD-1931 treatment reduced proliferation and viability in both cell types, but only at relatively high concentrations (*Eμ-Myc*, IC_{50} = 1.0μM, 95% CI 0.61–1.6 μM; HoxA9-Meis1 IC_{50} = 3.8 μM, 95% CI 1.2–12 μM).

To identify genetic factors that potentiate the cytotoxic action of molnupiravir on host cells, we performed genome-wide CRISPR/Cas9 screens in two independent *Eμ-Myc* lymphoma cell lines, AH15A and AF47A (Figure 1A). Genomic DNA was collected from cells after each round of selection, then guide sequences were amplified by PCR and quantified by sequencing. Enrichment was calculated at the level of individual guides and summary statistics calculated for each gene (Figure 1B, Tables S1 and S2). After four rounds of selection, the most enriched sgRNAs in both cell lines targeted *uridine–cytidine kinase 2* (*Uck2*), a kinase involved in the pyrimidine salvage pathway that phosphorylates uridine and cytidine to uridine monophosphate (UMP) and cytidine monophosphate (CMP), respectively. Other candidate genes included *Cytidine/Uridine Monophosphate Kinase 1* (*Cmpk1*), *transformation related protein p53* (*Trp53*), *p53 upregulated modulator of apoptosis* (*Puma*) and *PP2Aalpha (PPP2R1A) And B55A (PPP2R2A) Interacting Phosphatase Regulator 1* (*Pabir1*) (Figure 1B). Guides against these genes were typically enriched during the first round of selection (Figure S1A–E).

To validate the screen findings, we manipulated the functional activity of Uck2 in *Eμ-Myc* lymphoma cell lines, using CRISPR to inactivate the gene, or an exogenous expression vector to raise its activity, and tested response to EIDD-1931. We generated single cell clones with deleterious mutations in either one or both copies of *Uck2* and found that these lines were more resistant to EIDD-1931. The IC_{50} value for EIDD-1931 increased from 1.3 μM (95% CI 1.1–1.6 μM) in parental *Eμ-Myc* lymphoma cells to 3.4 μM (95% CI 1.8–6.6 μM) in *Uck2* heterozygous cells, but the resistance was more profound in cells that completely lacked functional Uck2 (IC_{50} not reached, >10 μM) (Figure 1C, Table S3). Exogenous expression of Uck2 sensitised cells to treatment with EIDD-1931, with a decrease in IC_{50} to 0.36 μM (95% CI 0.23–0.56 μM) (Figure 1C). Consistent results were obtained with HoxA9-Meis1 myeloid cell lines, where inactivation of *Uck2* produced a marked increase in the IC_{50} for EIDD-1931 (Figure 1D). Western blotting was used to confirm altered expression of Uck2 protein in both models (Figure 1E, Figure S1F, G). Additional smaller molecular weight products were detected in HoxA9-Meis1 myeloid cells expressing 3xFLAG-Uck2, which were not present when cells were lysed with pro-

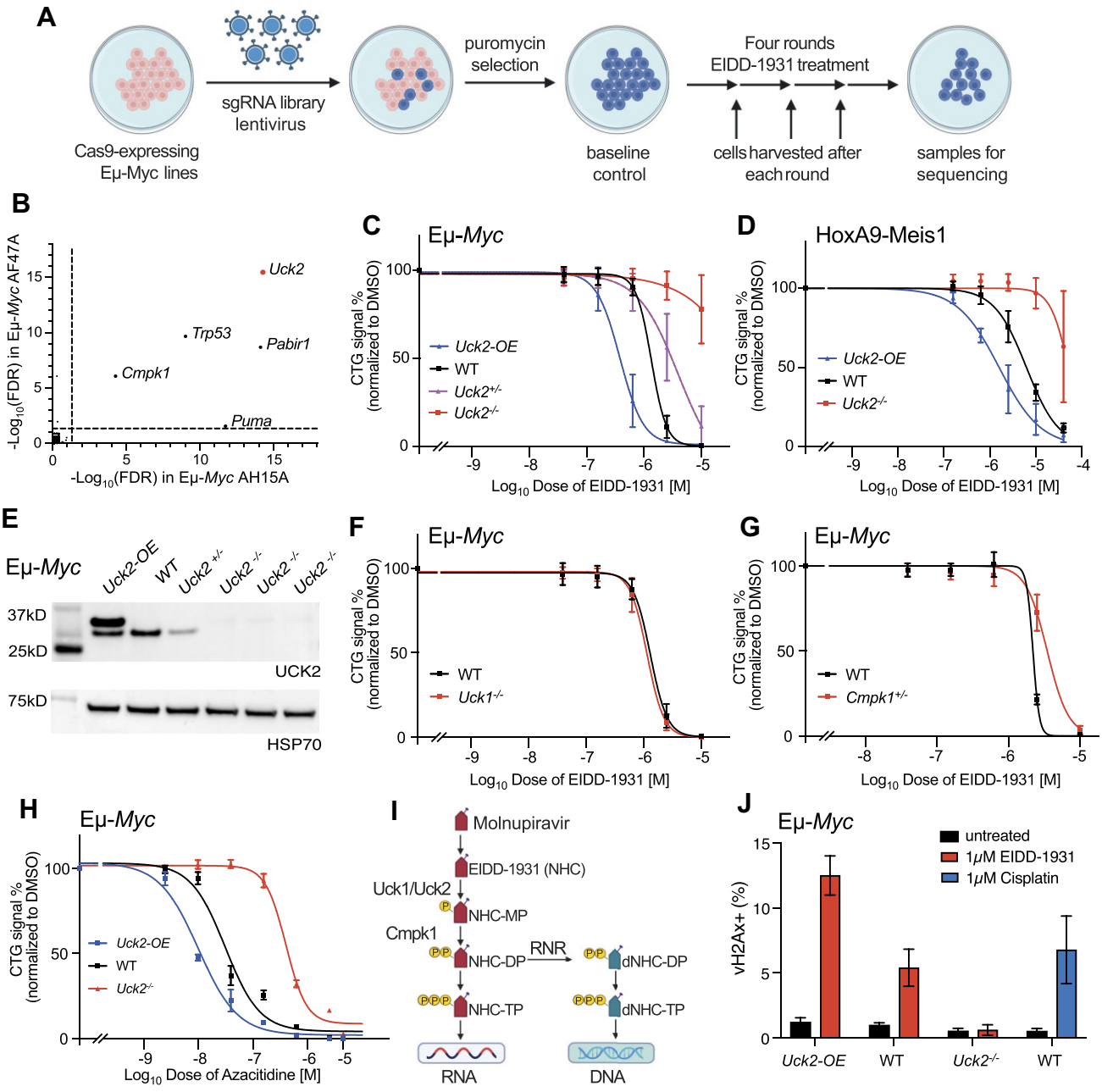

Figure 1. Identification of genetic factors that modify response to EIDD-1931. (**A**) Schematic of the CRISPR/Cas9 screens to identify genes that modulate EIDD-1931 response. (**B**) Gene level summary of guide enrichment in two *Eμ-Myc* lymphoma cell lines (AH15A and AF47A) selected with 5 μM EIDD-1931 over 4 rounds. The representation of the guides (4–5 per gene) was compared to baseline (day 3) and shown on a plot of -Log10 False Discovery Rate (FDR). Dotted lines mark an FDR value of 0.05. *Uck2* (in red) had the lowest FDR values in both lines. Impact of *Uck2* overexpression and loss on the sensitivity to EIDD-1931 in *Eμ-Myc* lymphoma cell lines (**C**) and HoxA9-Meis1 myeloid cell lines (**D**). (**E**) Immunoblots for Uck2 in *Uck2*-OE, WT, Uck2$^{+/-}$ and Uck2$^{-/-}$ *Eμ-Myc* lymphoma cell lines. HSP70 serves as a loading control. CellTiter-Glo assays were used to assess the impact of homozygous loss of *Uck1* (**F**) or heterozygous loss of *Cmpk1* (**G**) on the sensitivity of *Eμ-Myc* lymphoma cell lines to EIDD-1931. (**H**) Impact of Uck2 on the sensitivity of *Eμ-Myc* lymphoma cell lines to azacitidine. (**I**) Overview of ribonucleoside processing and contribution to RNA and DNA synthesis. (**J**) γ-H2AX staining analysis of *Uck2* over-expressing, parental *Eμ-Myc* lymphoma cells and isogenic Uck2$^{-/-}$ derivatives treated with 1 μM EIDD-1931 for 24 h. Parental cells treated with 1 μM Cisplatin for 24 h were used as a control. The positive cell fraction was determined based on gating on the untreated parental control. Data shown in C, D, F, G, H and J are means ± 1 SD from multiple replicate wells across 3–5 independent experiments, taken at 48 h (C,D,F and G) or 24h (H and J). Three independent CRISPR/Cas9 edited clones were used for *Uck2*$^{-/-}$ (C and D) and *Cmpk1*$^{+/-}$ (G), whereas two independent clones were used for other genotypes in C, D, F and H. Some parental (WT) control data are shared between C and F.

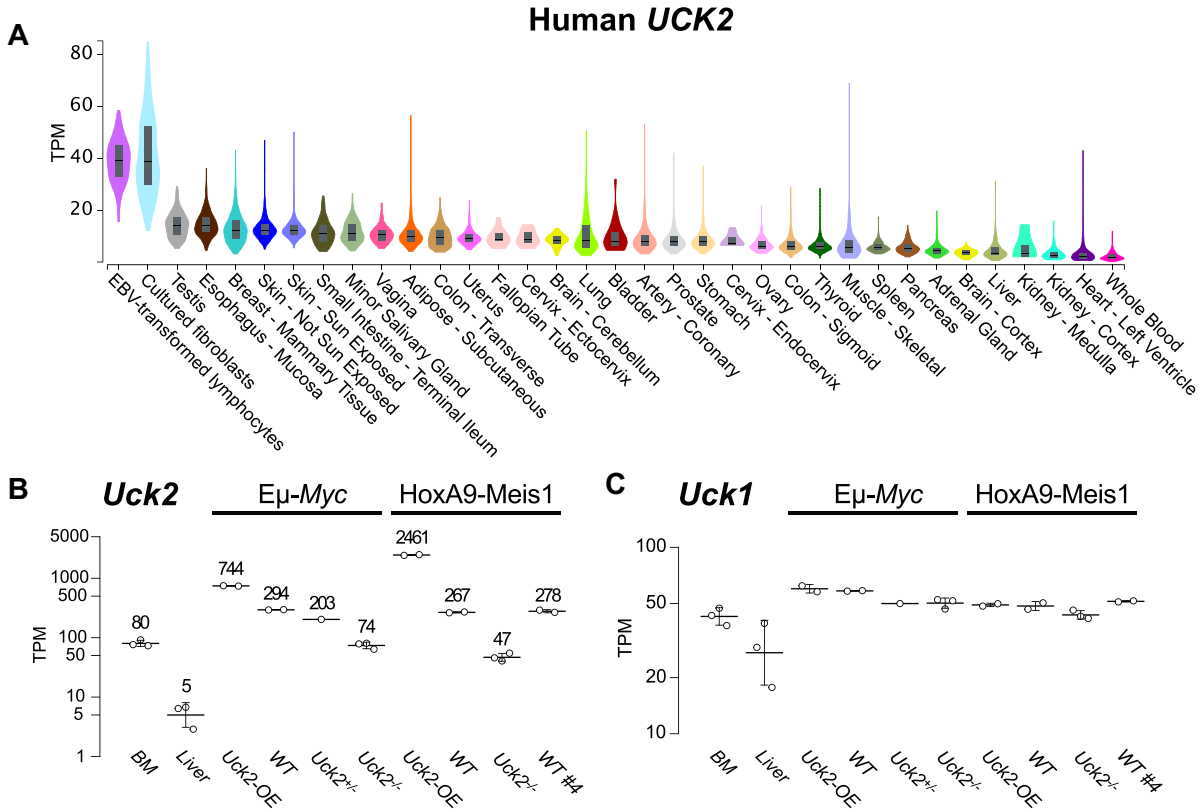

Figure 2. Assessment of uridine cytidine kinase expression. (**A**) Expression of *UCK2* in select human tissues and cells profiled by GTEx shown as Transcripts Per Million (TPM). Tissues were sorted based on the median expression. Box plots show the median and the 25th and 75th percentiles. Colour reflects the tissue, with labels at the bottom. The original plot was sourced from the GTEx portal then the text size and figure proportions were adjusted. Expression of mouse *Uck2* (**B**) and *Uck1* (**C**) in RNA-Seq performed using primary mouse tissues (n = 3 mice for each) and cell lines. Expression was assessed in the parental *Eμ-Myc* and HoxA9-Meis1 cell lines, CRISPR-edited derivatives and those expressing exogenous *Uck2*. A logarithmic scale was used for (B) and (C); geometric mean and standard deviation were calculated and the values for *Uck2* TPM values are displayed, rounded to the nearest whole number. Each point reflects an independent RNA extraction. WT#4 is an independent HoxA9-Meis1 cell line.

tein sample buffer (Figure S1F, G). This suggests that protease mediated degradation occurs in the myeloid cell line after lysis. Inactivation of *Uck1*, the other member of the uridine–cytidine kinase family, had no impact on the response to EIDD-1931 in Eμ-*Myc* lymphoma cells (Figure 1F). *Cmpk1*, which encodes a kinase that acts downstream of Uck2, also emerged as a candidate resistance gene. *Cmpk1* is an essential gene and CRISPR-mediated editing produced multiple single cell clones that retained a wildtype allele (31). Loss of one copy of *Cmpk1* induced some modest resistance to EIDD-1931 in Eμ-*Myc* cells (Figure 1G, Table S3). Prior work has shown that Uck2 can phosphorylate the hypomethylating agent azacytidine, a ribonucleoside analogue, and that this sensitises cancer cells to the drug (32,33). Altering Uck2 expression modified response to azacytidine in *Eμ-Myc* lymphoma cell lines (Figure 1H), but it did not impact response to decitabine, the deoxyribose form of azacytidine (Figure S1H). Collectively, these results are consistent with Uck2 exhibiting specificity for ribonucleoside analogs, including both azacytidine and EIDD-1931 (Figure 1I, Figure S2).

Trp53/p53 is a key tumour suppressor that plays a central role in coordinating the DNA damage response (34). We confirmed that loss of *Trp53* attenuated cytotoxicity from EIDD-1931 in both *Eμ-Myc* lymphoma cell lines and in HoxA9-Meis1 myeloid cells, but the overall shift in IC_{50} was modest (Figure S1I, J). EIDD-1931 treatment did not result in strong induction of Trp53 in either model after 24 h of treatment, which contrasted results when these cells were treated with the Mdm2 inhibitor Nutlin, or the DNA damaging agent etoposide (Figure S1K, L). Using flow intra-cellular staining and cytometric analysis, we found that levels of γ-H2AX increased in response to EIDD-1931 treatment in both cell types, and this was reduced in Uck2 deficient cells (Figure 1J, Figures S1M and S3).

Assessing the role of Uck2 in modifying the genotoxicity of EIDD-1931

UCK2 is thought to be lowly expressed in normal tissues, but is often upregulated in cell lines and cancers, including cancers from the lung, breast and liver (14,35–38). Expression profiling in the genotype-tissue expression (GTEx) atlas also supports this view, as *UCK2* expression is much higher in the two cultured tissues, EBV-transformed lymphocytes and fibroblasts (Figure 2A). Similarly, we found that expression of *Uck2* was higher in *Eμ-Myc* lymphoma and HoxA9-Meis1 myeloid cell lines than in bone marrow, and it was markedly elevated compared to liver (Figure 2B, Table S4). Introduction of loss of function mutations by CRISPR lowered *Uck2* expression, likely as a result of nonsense mediated decay (Figure 2B). Expression of *Uck1* was more consistent and was similar between cell lines and tissues (Figure 2C).

We went on to assess whether altering the expression of *Uck2* would influence the mutagenicity of NHC/EIDD-1931. To do this, HoxA9-Meis1 myeloid cells with varied expression of *Uck2* were treated with 1 μM EIDD-1931. Both the parental (wildtype, WT) and Uck2-deficient cells (Uck2-KO) tolerated this dose of drug, with doubling times increasing only modestly in the parental line, whereas growth of cells over expressing Uck2 (Uck2-OE) slowed and cell viability decreased markedly (Figure S4). For the mutagenicity assessment, cells were treated with 1 μM EIDD-1931 twice for four days at a time, with three days recovery between treatments (Figure 3A). Single cell clones were then isolated from each condition; these cells were expanded, protein levels assessed (Figure S5A) and DNA isolated for genome sequencing. The average read depth over the non-repeat genome for the single cell clones was 32 ± 7.5 (range 16–40) (Table S5). Mutation rates were adjusted to account for variable coverage and were expressed as mutations per megabase pair (Mbp). EIDD-1931 treatment was associated with a significant increase in the rate of single base substitutions (SBSs) in HoxA9-Meis1 myeloid cells (WT average DMSO = 0.32 ± 0.03 SBS/Mbp and EIDD-1931 = 0.97 ± 0.03 SBS/Mbp) (Figure 3B). When we examined the mutational spectra, it was clear that the increase in mutations was predominantly T > C mutations and to a lesser extent C > T mutations (Figure 3C, Figure S5B, Tables S6 and S7). EIDD-1931 treatment was associated with an even higher mutation burden in cells exogenously expressing Uck2, with a 59 ± 23% increase of the total SBS mutation rate beyond wildtype cells treated with EIDD-1931 (Uck2-OE average DMSO = 0.37 ± 0.09 SBS/Mbp, average EIDD-1931 = 1.54 ± 0.23 SBS/Mbp) (Figure 3B). In contrast, inactivation of Uck2 lessened the mutagenic influence of EIDD-1931 treatment (Figure 3B). We observed no change in the frequency of insertions and deletions (indels) in response to EIDD-1931 treatment (Figure 3B), nor was there any obvious increase in copy number variants, irrespective of the level of Uck2 expression (Figure S5C).

To better define the SBS mutational signature linked to treatment with EIDD-1931, we calculated a background signature to reflect the mutational processes in HoxA9-Meis1 myeloid cells. The background signature was subtracted from EIDD-1931 treated conditions to generate a refined EIDD-1931 signature (Figure 4A, Table S8). Using the same approach, we derived SBS signatures from human and mouse cell lines treated with EIDD-1931 or molnupiravir (10) and found these were highly concordant with our refined EIDD-1931 signature, with cosine similarities between 0.93 and 0.99 (Figure 4B, Figure S6). We also used non-negative matrix factorisation to derive SBS signatures from HoxA9-Meis1 samples de novo and identified the same background and EIDD-1931 associated signatures with cosine similarities 0.97–0.99 (Figure 4C, Figure S7). We calculated the mutation rate for each signature in our samples (Figure 4D, Table S9). Using this approach, we classified an average of 1308 ± 243 mutations linked to EIDD-1931 in wildtype cells, representing a rate of 0.59 ± 0.11 mutations per Mbp. The rate increased to 1.18 ± 0.18/Mbp in Uck2-OE cells and dropped to 0.05 ± 0.02/Mbp in Uck2-KO cells (Figure 4D). While the mutation rate attributable to EIDD-1931 was low in Uck2-KO cells, roughly 8% of that seen in wildtype cells, the signal was still elevated compared to cells treated with DMSO (means range between 2.0 and 6.1 × 10^{-3}/Mbp) although this difference was not statistically significant.

We also compared the EIDD-1931 signature to established SBS signatures from COSMIC, but no highly similar signatures were found. SBS12 and 37 were the most similar, with cosine similarity of 0.71 and 0.69, respectively (Figure S8A). The EIDD-1931 signature had a tri-nucleotide context preference of WTY (W = T or A, Y = T or C), but we did not see evidence of strong bias beyond this trimer (Figure S8B). Looking at other features of the signature, there was some minor depletion of T > C mutations on the transcribed strand, but the absolute difference was modest (Figure S8C-D).

Discussion

Molnupiravir is designed to disrupt viral replication through its potent mutagenic activity—a strategy defined as lethal mutagenesis (39,40). This strategy is not without risk, both in terms of the potential to accelerate sequence diversification within the virus, but also because of the potential for collateral damage to the host genome. Molnupiravir and NHC/EIDD-1931 both induce mutations in bacteria in the Ames test (12,13), and they elevate mutation rates in human and mouse cell lines (10,11). Yet these results sit in contrast to *in vivo* safety testing performed in mice and rats, which failed to detect evidence of genotoxicity or carcinogenicity (12,13). By applying unbiased genetic screens we have found that expression of the pyrimidine salvage pathway component Uck2 potentiates the cytotoxicity and mutagenicity of EIDD-1931 in mouse cell lines. Uck2 shows low and variable expression in normal tissues (14), but it is upregulated in many cancers and cell lines and this difference may reconcile inconsistent findings regarding the mutagenicity of molnupiravir and NHC/EIDD-1931 in different experimental systems.

We explored the toxicity and mutagenicity of NHC using murine blood cancer derived cell lines. NHC treatment in HoxA9-Meis1 myeloid cells was cytotoxic and drove an increase in somatic mutation burden, with a distinctive mutational signature enriched for T:A to C:G transitions. This mirrors prior work with NHC and molnupiravir in human and mouse cell lines, with highly concordance of mutational signatures produced across studies (Figure 4B, Figure S6). Yet the findings appear to be at odds with the safety evaluation of molnupiravir, where genotoxicity assays failed to detect mutagenesis beyond background levels in rats, despite evaluating higher doses of molnupiravir over a longer period (e.g. 500 mg/kg/day for four weeks) (12,13). For cell lines, low levels of NHC, between 0.26 and 0.5 μg/ml given over 5–8 days, appear sufficient to induce toxicity and mutations. These exposures likely sit at the low end of what people would experience during treatment for SARS-Cov2, where 800 mg of molnupiravir is given twice daily for five days and NHC concentrations in the plasma on day 1 peak at ∼3.5 μg/ml (4,41). These findings suggest that cell lines are more sensitive to the mutagenic influence of molnupiravir and NHC and, therefore, estimates of mutagenicity from cell lines may be inflated compared to normal tissues.

Just like their native counterparts, ribonucleoside analogs, such as NHC, must be phosphorylated through the mono-, di- and tri-phosphate forms before they can be incorporated into RNA. Phosphorylation of a ribonucleoside (or its analog) also enables entry into the nucleotide pool, via the action of ribonucleotide reductase, and subsequent incorporation into DNA (Figure 1I). Our results are consistent with Uck2 being the primary kinase responsible for the initial phos-

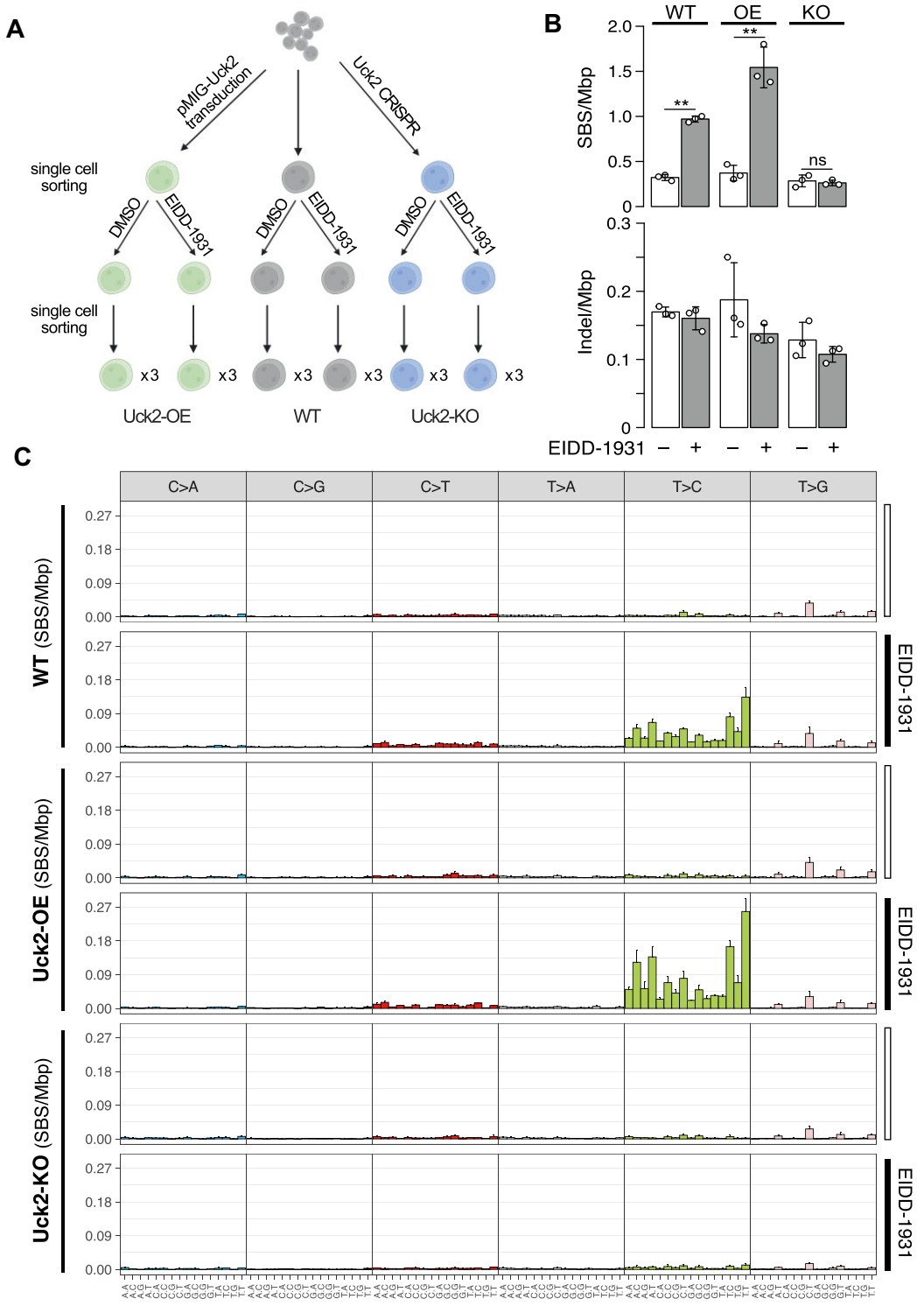

Figure 3. Somatic mutation profiling following treatment with NHC/EIDD-1931. (**A**) Experimental outline for evaluating NHC/EIDD-1931 induced mutagenesis and the influence of Uck2. Murine HoxA9-Meis1 myeloid cell lines were generated to express varied levels of Uck2: Parental (WT), over-expressed (OE) or CRISPR knockout (KO). Cells were exposed to EIDD-1931 in culture before single cell cloning and genome sequencing. (**B**) Absolute mutation rates were calculated for SBS (at top) and for insertions and deletions (indels, at bottom). Each data point represents a clone, error bars show the standard deviation. An ANOVA and pairwise comparison was performed to compare between DMSO and EIDD-1931 treated clones, asterisks denote a significant difference (** $P < 0.0001$). (**C**) Mutational spectra are shown, detailing the mutation rate as the number of mutations per megabase for each substitution (SBS/Mbp). The mutational spectra in this figure are not normalised for genome-wide trimer abundance. Three single cell clones were analysed for each condition; the mean is plotted with the standard deviation.

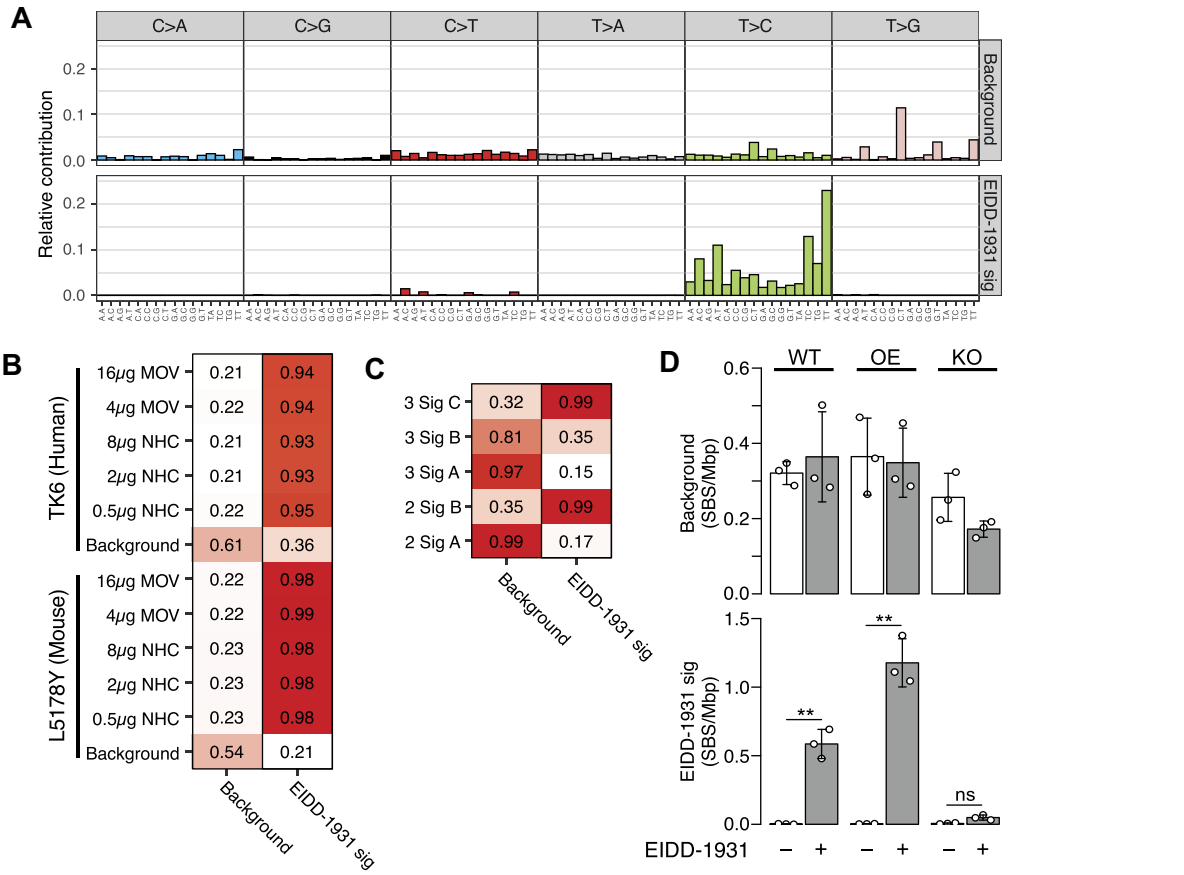

Figure 4. Derivation and quantification of an EIDD-1931 SBS signature. (**A**) Background and EIDD-1931 signatures were derived from HoxA9-Meis1 myeloid cell lines. Our derived SBS signatures were compared to those derived from TK6 (human) or L5178Y (mouse) cell lines treated with molnupiravir (MOV) or NHC (10) (**B**), or to signatures derived de novo considering two (2 Sig A/B) or three (3 Sig A/B/C) signature outputs (**C**). Heatmaps shows the cosine similarity, with a colour gradient from white to red (1). (**D**) Quantification of the background (at top) or EIDD-1931 signature (bottom) in genome sequencing data from HoxA9-Meis1 cell lines. Each datapoint represents a clone and the mean and standard deviation is shown. An ANOVA and pairwise comparison was performed to compare between DMSO and EIDD-1931 treated clones, asterisks denote a significant difference (** $P < 0.0001$).

phorylation of NHC in the two cancer cell lines tested. This is not surprising, as UCK2 has greater catalytic activity than UCK1 (estimated at 15- to 20-fold higher) and may have broader substrate specificity (14). In the absence of Uck2 we saw a marked reduction in the mutagenic activity of NHC in HoxA9-Meis1 myeloid cells. While the mutation rate was consistently higher in Uck2-deficient cells upon NHC treatment, the change was not statistically significant. Our experiment assessed three clones per condition and was not designed to detect subtle changes in mutation burden. The fact molnupiravir is active as an antiviral is an indication that NHC is phosphorylated and enters the ribonucleotide pool in cells, but it may be that in the absence of UCK2 it does not reach sufficient levels to induce a high number of mutations. It is notable that the tissues assessed in the genotoxicity assays, blood and liver, have relatively low *UCK2* expression when compared with other tissues or cultured cells (Figure 2). At least this could explain why the drug did not return a positive result in genotoxicity assays, but it also suggests further work is required to assess and quantify any impact of the treatment on normal tissues, using larger sample sizes, or more sensitive approaches, including error-corrected or high-fidelity sequencing (10).

The aberrant expression of UCK2 has been exploited as a strategy to target cancer cells with ribonucleoside analogs (reviewed in (15)). Indeed, UCK2 expression is a major determinant of response for a broad array of ribonucleoside analogs, including azacytidine (32,33), fluorocyclopentenylcytosine (42) and 3′-ethynyl nucleosides (43). Relatively little is known about the factors that regulate UCK2 expression in normal tissues or in cancers, but this warrants further attention. Our results suggest that molnupiravir or NHC could elevate the rate of mutagenesis in cancer cells with some degree of selectivity. While this could potentially be exploited as a therapeutic strategy, it also raises the prospect that cancers exposed to molnupiravir will accumulate mutations that could contribute to disease progression or therapy resistance. It should be possible to test this by looking for the EIDD-1931 mutational signature in cancers that develop after treatment with molnupiravir. This strategy has been applied to study mutations linked to other antivirals (44,45). We also identified p53 as a factor that can modulate response to NHC treatment, even though the drug did not appear to trigger p53 induction (Figure S1). It may be that loss of p53 dampens the stress response or raises the apoptotic threshold in these cells (46), or it could indicate some change in how the drug is being metabolised (47), but this remains to be determined. Nonetheless, these findings highlight how underlying genetic, transcriptional and metabolic differences may result in variable drug activity and suggest caution when using cell lines alone to assess the mutagenic activity of new treatments.

It is important to point out the differences between testing for mutagenicity in a research environment as compared to a safety evaluation for a regulator. Firstly, our study is restricted to the *in vitro* assessment of mouse blood cancer derived cell lines, whereas the safety evaluation involved treatment in different animal models, at various developmental stages and explored a wide range of doses and treatment periods (12,13). It is possible that tissue and species differences, or the biology of any individual cell line, would impact the activity of the drug or its turnover. Secondly, we have directly treated the cells with the active component of the drug, NHC/EIDD-1931, which is different to oral administration of molnupiravir. Our treatment of the cell lines was for eight days, and included a rest period to avoid unwanted toxicity, which does not match the clinical treatment course. Our work could be strengthened by performing *in vivo* drug treatments that more closely mirror the prescribed dosing schedule, and would benefit from the assessment of both normal tissues and cancers, which could be achieved by treating mice grafted with cancer cell lines. We did observe changes in the rate of cell growth across genotypes, particularly in response to EIDD-1931 treatment, and further work is required to understand how this might impact the assessment of mutagenicity. Lastly, our evaluation is on transformed cells, rather than a primary tissue. Some of these points were raised in response to the initial description of mutagenic activity of molnupiravir in cell lines (11,48). Now that these findings have been replicated by independent laboratories, we have no reason to doubt that administration of molnupiravir or NHC can induce mutations in some mouse and human cancer cell lines (10,11). Our findings suggest that altered metabolic activity in cancer cell lines, specifically high-level expression of Uck2/UCK2, may explain why it is that these results are not reflective of the mutagenic activity of molnupiravir in primary tissues.

Drugs that disrupt DNA and RNA synthesis feature among our most essential medicines. There are various strategies available to try and enhance the selectivity of these agents to avoid toxic impacts on normal tissues. For antivirals, this may include exploiting differences between the host and pathogen, or if the drug acts broadly, it will typically rely on the higher toxic burden a mutation imposes on a pathogen's genome, because of its smaller size. While we have not tested primary tissues in this work, our results suggest that NHC could potentially have some low-level mutagenic activity towards the host genome, but that this would be enhanced in cells that activate the pyrimidine salvage pathway, which is a common feature in cancers and cancer-derived cell lines. It may be that UCK2-deficient cells provide a model for testing for mutagenic activity for ribonucleoside analogs that is more indicative of performance in a proliferative tissue. However, our results caution against over reliance on cell lines for assessing mutagenic activity, and we encourage broader *in vivo* assessment of these drugs in model systems, across various tissues and in different contexts (e.g. across developmental stages, in metabolic disorders or with combination treatments), to account for different metabolic states and for other factors that could impact activity.

Data availability

Genome sequencing data from the HoxA9-Meis1 cell lines (accession: PRJNA950474), amplicon sequence from the CRISPR/Cas9 screen (accession: PRJNA950560) and RNA-Seq for expression analysis (accession: PRJNA1014119) are available in the Sequence Read Archive. Processed datasets are provided in the supplementary materials and code used to generate figure elements is provided in figshare at https://doi.org/10.6084/m9.figshare.24312733.

Supplementary data

Supplementary Data are available at NAR Online.

Acknowledgements

We would like to thank our colleagues for useful discussions during preparation of the manuscript. The manuscript made use of data from The Genotype-Tissue Expression (GTEx) Project. GTEx was supported by the Common Fund of the Office of the Director of the National Institutes of Health, and by NCI, NHGRI, NHLBI, NIDA, NIMH, and NINDS. The data used for the analyses described in this manuscript were first obtained from the GTEx Portal on 24 March 2023 then updated on 22 August 2023. Figure 1I was created with BioRender.com.

Author contributions: Zhen Xu: Conceptualization, Data curation, Investigation, Software, Writing—original draft, Writing—review & editing. Christoffer Flensburg: Data curation, Investigation, Software, Writing—original draft, Writing—review & editing. Rebecca Bilardi: Investigation, Writing—review & editing. Ian Majewski: Conceptualization, Supervision, Writing—original draft, Writing—review & editing.

Funding

Victorian State Government Operational Infrastructure Support and Australian Government NHMRC IRIISS. Funding for open access charge: Institutional funding.

Conflict of interest statement

None declared.

References

1. Jayk Bernal,A., Gomes da Silva,M.M., Musungaie,D.B., Kovalchuk,E., Gonzalez,A., Delos Reyes,V., Martin-Quiros,A., Caraco,Y., Williams-Diaz,A., Brown,M.L., *et al.* (2022) Molnupiravir for oral treatment of Covid-19 in nonhospitalized patients. *N. Engl. J. Med.*, **386**, 509–520.
2. Khoo,S.H., FitzGerald,R., Saunders,G., Middleton,C., Ahmad,S., Edwards,C.J., Hadjiyiannakis,D., Walker,L., Lyon,R., Shaw,V., *et al.* (2023) Molnupiravir versus placebo in unvaccinated and vaccinated patients with early SARS-CoV-2 infection in the UK (AGILE CST-2): a randomised, placebo-controlled, double-blind, phase 2 trial. *Lancet Infect. Dis.*, **23**, 183–195.
3. Butler,C.C., Hobbs,F.D.R., Gbinigie,O.A., Rahman,N.M., Hayward,G., Richards,D.B., Dorward,J., Lowe,D.M., Standing,J.F., Breuer,J., *et al.* (2023) Molnupiravir plus usual care versus usual care alone as early treatment for adults with COVID-19 at increased risk of adverse outcomes (PANORAMIC): an open-label, platform-adaptive randomised controlled trial. *Lancet*, **401**, 281–293.
4. Painter,W.P., Holman,W., Bush,J.A., Almazedi,F., Malik,H., Eraut,N., Morin,M.J., Szewczyk,L.J. and Painter,G.R. (2021) Human safety, tolerability, and pharmacokinetics of molnupiravir,

a novel broad-spectrum oral antiviral agent with activity against SARS-CoV-2. *Antimicrob. Agents Chemother.*, **65**, e02428-20.
5. Agostini,M.L., Pruijssers,A.J., Chappell,J.D., Gribble,J., Lu,X., Andres,E.L., Bluemling,G.R., Lockwood,M.A., Sheahan,T.P., Sims,A.C., *et al.* (2019) Small-molecule antiviral beta-d-N(4)-hydroxycytidine inhibits a proofreading-intact coronavirus with a high genetic barrier to resistance. *J. Virol.*, **93**, e01348-19.
6. Arribas,J.R., Bhagani,S., Lobo,S.M., Khaertynova,I., Mateu,L., Fishchuk,R., Park,W.Y., Hussein,K., Kim,S.W., Ghosn,J., *et al.* (2022) Randomized trial of molnupiravir or placebo in patients hospitalized with Covid-19. *NEJM Evidence*, **1**, EVIDoa2100044.
7. Caraco,Y., Crofoot,G.E., Moncada,P.A., Galustyan,A.N., Musungaie,D.B., Payne,B., Kovalchuk,E., Gonzalez,A., Brown,M.L., Williams-Diaz,A., *et al.* (2022) Phase 2/3 Trial of molnupiravir for treatment of Covid-19 in nonhospitalized adults. *NEJM Evidence*, **1**, EVIDoa2100043.
8. Sheahan,T.P., Sims,A.C., Zhou,S., Graham,R.L., Pruijssers,A.J., Agostini,M.L., Leist,S.R., Schafer,A., Dinnon,K.H., Stevens,L.J., *et al.* (2020) An orally bioavailable broad-spectrum antiviral inhibits SARS-CoV-2 in human airway epithelial cell cultures and multiple coronaviruses in mice. *Sci. Transl. Med.*, **12**, eabb5883.
9. Waters,M.D., Warren,S., Hughes,C., Lewis,P. and Zhang,F. (2022) Human genetic risk of treatment with antiviral nucleoside analog drugs that induce lethal mutagenesis: the special case of molnupiravir. *Environ. Mol. Mutagen.*, **63**, 37–63.
10. Miranda,J.A., McKinzie,P.B., Dobrovolsky,V.N. and Revollo,J.R. (2022) Evaluation of the mutagenic effects of molnupiravir and N4-hydroxycytidine in bacterial and mammalian cells by HiFi sequencing. *Environ. Mol. Mutagen.*, **63**, 320–328.
11. Zhou,S., Hill,C.S., Sarkar,S., Tse,L.V., Woodburn,B.M.D., Schinazi,R.F., Sheahan,T.P., Baric,R.S., Heise,M.T. and Swanstrom,R. (2021) beta-d-N4-hydroxycytidine Inhibits SARS-CoV-2 through lethal mutagenesis but is also mutagenic to mammalian cells. *J. Infect. Dis.*, **224**, 415–419.
12. United Kingdom Medicines and Healthcare products Regulatory Agency (UK MHRA) (2021) Public Assessment Report - Lagevrio 200 mg hard capsules (molnupiravir) PLGB 53095/0089. Nov 4, 2021.
13. United States Food and Drug Administration (US FDA) (2021) FDA Briefing Document: Antimicrobial Drugs Advisory Committee Meeting. Nov 30, 2021.
14. Van Rompay,A.R., Norda,A., Linden,K., Johansson,M. and Karlsson,A. (2001) Phosphorylation of uridine and cytidine nucleoside analogs by two human uridine–cytidine kinases. *Mol. Pharmacol.*, **59**, 1181–1186.
15. Fu,Y., Wei,X.D., Guo,L., Wu,K., Le,J., Ma,Y., Kong,X., Tong,Y. and Wu,H. (2022) The metabolic and non-metabolic roles of UCK2 in tumor progression. *Front. Oncol.*, **12**, 904887.
16. Kelly,G.L., Grabow,S., Glaser,S.P., Fitzsimmons,L., Aubrey,B.J., Okamoto,T., Valente,L.J., Robati,M., Tai,L., Fairlie,W.D., *et al.* (2014) Targeting of MCL-1 kills MYC-driven mouse and human lymphomas even when they bear mutations in p53. *Genes Dev.*, **28**, 58–70.
17. Kroon,E., Krosl,J., Thorsteinsdottir,U., Baban,S., Buchberg,A.M. and Sauvageau,G. (1998) Hoxa9 transforms primary bone marrow cells through specific collaboration with Meis1a but not Pbx1b. *EMBO J.*, **17**, 3714–3725.
18. Koike-Yusa,H., Li,Y., Tan,E.P., Velasco-Herrera Mdel,C. and Yusa,K. (2014) Genome-wide recessive genetic screening in mammalian cells with a lentiviral CRISPR-guide RNA library. *Nat. Biotechnol.*, **32**, 267–273.
19. Aubrey,B.J., Kelly,G.L., Kueh,A.J., Brennan,M.S., O'Connor,L., Milla,L., Wilcox,S., Tai,L., Strasser,A. and Herold,M.J. (2015) An inducible lentiviral guide RNA platform enables the identification of tumor-essential genes and tumor-promoting mutations in vivo. *Cell Rep.*, **10**, 1422–1432.
20. Eden,E., Lipson,D., Yogev,S. and Yakhini,Z. (2007) Discovering motifs in ranked lists of DNA sequences. *PLoS Comput. Biol.*, **3**, e39.
21. Dobin,A., Davis,C.A., Schlesinger,F., Drenkow,J., Zaleski,C., Jha,S., Batut,P., Chaisson,M. and Gingeras,T.R. (2013) STAR: ultrafast universal RNA-seq aligner. *Bioinformatics*, **29**, 15–21.
22. Liao,Y., Smyth,G.K. and Shi,W. (2014) featureCounts: an efficient general purpose program for assigning sequence reads to genomic features. *Bioinformatics*, **30**, 923–930.
23. Li,H. (2013) Aligning sequence reads, clone sequences and assembly contigs with BWA-MEM. arXiv doi: https://doi.org/10.48550/arXiv.1303.3997, 16 March 2013, preprint: not peer reviewed.
24. Flensburg,C., Sargeant,T., Oshlack,A. and Majewski,I.J. (2020) SuperFreq: integrated mutation detection and clonal tracking in cancer. *PLoS Comput. Biol.*, **16**, e1007603.
25. Koboldt,D.C., Zhang,Q., Larson,D.E., Shen,D., McLellan,M.D., Lin,L., Miller,C.A., Mardis,E.R., Ding,L. and Wilson,R.K. (2012) VarScan 2: somatic mutation and copy number alteration discovery in cancer by exome sequencing. *Genome Res.*, **22**, 568–576.
26. Lilue,J., Doran,A.G., Fiddes,I.T., Abrudan,M., Armstrong,J., Bennett,R., Chow,W., Collins,J., Collins,S., Czechanski,A., *et al.* (2018) Sixteen diverse laboratory mouse reference genomes define strain-specific haplotypes and novel functional loci. *Nat. Genet.*, **50**, 1574–1583.
27. Blokzijl,F., Janssen,R., van Boxtel,R. and Cuppen,E. (2018) MutationalPatterns: comprehensive genome-wide analysis of mutational processes. *Genome. Med.*, **10**, 33.
28. Costello,M., Pugh,T.J., Fennell,T.J., Stewart,C., Lichtenstein,L., Meldrim,J.C., Fostel,J.L., Friedrich,D.C., Perrin,D., Dionne,D., *et al.* (2013) Discovery and characterization of artifactual mutations in deep coverage targeted capture sequencing data due to oxidative DNA damage during sample preparation. *Nucleic Acids Res.*, **41**, e67.
29. Gaujoux,R. and Seoighe,C. (2010) A flexible R package for nonnegative matrix factorization. *BMC Bioinf.*, **11**, 367.
30. Adams,J.M., Harris,A.W., Pinkert,C.A., Corcoran,L.M., Alexander,W.S., Cory,S., Palmiter,R.D. and Brinster,R.L. (1985) The c-myc oncogene driven by immunoglobulin enhancers induces lymphoid malignancy in transgenic mice. *Nature*, **318**, 533–538.
31. Tzelepis,K., Koike-Yusa,H., De Braekeleer,E., Li,Y., Metzakopian,E., Dovey,O.M., Mupo,A., Grinkevich,V., Li,M., Mazan,M., *et al.* (2016) A CRISPR dropout screen identifies genetic vulnerabilities and therapeutic targets in acute myeloid leukemia. *Cell Rep.*, **17**, 1193–1205.
32. Gruber,E., Franich,R.L., Shortt,J., Johnstone,R.W. and Kats,L.M. (2020) Distinct and overlapping mechanisms of resistance to azacytidine and guadecitabine in acute myeloid leukemia. *Leukemia*, **34**, 3388–3392.
33. Sripayap,P., Nagai,T., Uesawa,M., Kobayashi,H., Tsukahara,T., Ohmine,K., Muroi,K. and Ozawa,K. (2014) Mechanisms of resistance to azacitidine in human leukemia cell lines. *Exp. Hematol.*, **42**, 294–306.
34. Kruiswijk,F., Labuschagne,C.F. and Vousden,K.H. (2015) p53 in survival, death and metabolic health: a lifeguard with a licence to kill. *Nat. Rev. Mol. Cell Biol.*, **16**, 393–405.
35. Huang,S., Li,J., Tam,N.L., Sun,C., Hou,Y., Hughes,B., Wang,Z., Zhou,Q., He,X. and Wu,L. (2019) Uridine-cytidine kinase 2 upregulation predicts poor prognosis of hepatocellular carcinoma and is associated with cancer aggressiveness. *Mol. Carcinog.*, **58**, 603–615.
36. Shen,G., He,P., Mao,Y., Li,P., Luh,F., Ding,G., Liu,X. and Yen,Y. (2017) Overexpression of uridine-cytidine kinase 2 correlates with breast cancer progression and poor prognosis. *J Breast Cancer*, **20**, 132–141.
37. Wu,Y., Jamal,M., Xie,T., Sun,J., Song,T., Yin,Q., Li,J., Pan,S., Zeng,X., Xie,S., *et al.* (2019) Uridine-cytidine kinase 2 (UCK2): a

potential diagnostic and prognostic biomarker for lung cancer. *Cancer Sci.*, **110**, 2734–2747.
38. Yu,S., Li,X., Guo,X., Zhang,H., Qin,R. and Wang,M. (2019) UCK2 upregulation might serve as an indicator of unfavorable prognosis of hepatocellular carcinoma. *IUBMB Life*, **71**, 105–112.
39. Anderson,J.P., Daifuku,R. and Loeb,L.A. (2004) Viral error catastrophe by mutagenic nucleosides. *Annu. Rev. Microbiol.*, **58**, 183–205.
40. Swanstrom,R. and Schinazi,R.F. (2022) Lethal mutagenesis as an antiviral strategy. *Science*, **375**, 497–498.
41. FitzGerald,R., Dickinson,L., Else,L., Fletcher,T., Hale,C., Amara,A., Walker,L., Penchala,S.D., Lyon,R., Shaw,V., *et al.* (2022) Pharmacokinetics of B-d-N4-hydroxycytidine, the parent nucleoside of prodrug molnupiravir, in nonplasma compartments of patients with severe acute respiratory syndrome coronavirus 2 infection. *Clin. Infect. Dis.*, **75**, e525–e528.
42. Sarkisjan,D., Julsing,J.R., Smid,K., de Klerk,D., van Kuilenburg,A.B., Meinsma,R., Lee,Y.B., Kim,D.J. and Peters,G.J. (2016) The cytidine analog fluorocyclopentenylcytosine (RX-3117) is activated by uridine-cytidine kinase 2. *PLoS One*, **11**, e0162901.
43. Murata,D., Endo,Y., Obata,T., Sakamoto,K., Syouji,Y., Kadohira,M., Matsuda,A. and Sasaki,T. (2004) A crucial role of uridine/cytidine kinase 2 in antitumor activity of 3'-ethynyl nucleosides. *Drug Metab. Dispos.*, **32**, 1178–1182.
44. de Kanter,J.K., Peci,F., Bertrums,E., Rosendahl Huber,A., van Leeuwen,A., van Roosmalen,M.J., Manders,F., Verheul,M., Oka,R., Brandsma,A.M., *et al.* (2021) Antiviral treatment causes a unique mutational signature in cancers of transplantation recipients. *Cell Stem Cell*, **28**, 1726–1739.
45. Fang,H., Yan,H.H.N., Bilardi,R.A., Flensburg,C., Yang,H., Barbour,J.A., Siu,H.C., Turski,M., Chew,E., Xu,Z., *et al.* (2022) Ganciclovir-induced mutations are present in a diverse spectrum of post-transplant malignancies. *Genome. Med.*, **14**, 124.
46. Aubrey,B.J., Strasser,A. and Kelly,G.L. (2016) Tumor-suppressor functions of the TP53 pathway. *Cold Spring Harb. Perspect. Med.*, **6**, a026062.
47. Vousden,K.H. and Ryan,K.M. (2009) p53 and metabolism. *Nat. Rev. Cancer*, **9**, 691–700.
48. Troth,S., Butterton,J., DeAnda,C.S., Escobar,P., Grobler,J., Hazuda,D. and Painter,G. (2021) Letter to the editor in response to Zhou et al. *J. Infect. Dis.*, **224**, 1442–1443.

Received: June 7, 2023. **Revised:** October 11, 2023. **Editorial Decision:** October 12, 2023. **Accepted:** October 19, 2023
© The Author(s) 2023. Published by Oxford University Press on behalf of Nucleic Acids Research.
This is an Open Access article distributed under the terms of the Creative Commons Attribution-NonCommercial License (http://creativecommons.org/licenses/by-nc/4.0/), which permits non-commercial re-use, distribution, and reproduction in any medium, provided the original work is properly cited. For commercial re-use, please contact journals.permissions@oup.com